Supplement: Parameterising secondary organic aerosol formation from α-pinene using a detailed oxidation and aerosol formation model

Karl Ceulemans, Steven Compernolle, Jean-François Müller

June 1, 2012

S1 Generic Chemistry: Description

S1.1 Generic species

The generic chemistry system was introduced in Capouet et al. (2008), and further extended in Ceulemans et al. (2010). Generic species are defined by their carbon number (from 10 down to 6) and by one explicit functional group. The generic species are further subdivided into 11 volatility classes. Each class represents lumped organic compounds, which have a 'parent compound' (the molecule resulting from replacement of the explicit functional group by one or more hydrogen atoms) with a saturated liquid vapour pressure $p^0_{\mathrm{L,parent}}$ falling within the volatility class range. For the highest volatility class, indicated by the letter 'a', $p^0_{\mathrm{L,parent}} > 10^{-1}$ Torr at 298 K. Class 'b' contains species with 10^{-1} Torr $> p^0_{\mathrm{L,parent}} > 10^{-1.5}$ Torr, etc., and for class 'k', $p^0_{\mathrm{L,parent}} < 10^{-5.5}$ Torr.

In our notation a generic species name consists of the prefix 'LX', the carbon number, the vapour pressure class symbol and the explicit functional group. In total there are 55 classes (5 carbon numbers times eleven vapour pressure classes), besides the generic products with less than 6 carbon atoms, which are not considered for SOA formation, and lumped into a special generic class (with prefix 'SX').

The vapour pressure of a (non-radical) generic species is determined by the contribution of its explicit group (see Table S1), and the representative volatility class vapour pressure $p^0_{\mathrm{L,LX}}$, which at 298 K is equal to the geometric mean of the volatility class range for classes 'b'-'j', $10^{-0.75}$ Torr for class 'a', and $10^{-5.75}$ Torr for class 'k'. The temperature dependence of $p^0_{\mathrm{L,LX}}$ is estimated based on Makar (2001).

Table S1: Overview of generic species.

Generic species	Explicitly represented group	$\Delta \log_{10} p^0_{\mathrm{group}}$ (Capouet and Müller, 2006)	Note
LX10eOOH	hydroperoxide	$-2.9942 + 0.0332(T - 298)$	
LX10eOH	alcohol	$-2.0374 + 0.0124(T - 298)$	
LX10eCHO	aldehyde	$-0.8937 + 0.0124(T - 298)$	a
LX10eCAR	keto-aldehyde	$-1.787 + 0.0248(T - 298)$	a
LX10eKET	ketone	$-0.8937 + 0.0124(T - 298)$	
LX10ePAN	peroxy acyl nitrate	$-2.5372 + 0.0113(T - 298)$	a,b
LX10eONO2	nitrate	$-1.6711 + 0.0063(T - 298)$	
LX10eCOOH	carboxylic acid	$-3.2516 + 0.0075(T - 298)$	a
LX10eCOOOH	peroxy acid	$-3.2516 + 0.0075(T - 298)$	a
LX10eO	alkoxy radical		
LX10eO2	peroxy radical		
LX10e03	acyl peroxy radical		

[a] The carbons in this explicit group are already accounted for in the implicit part of the species.
[b] The contribution of the PAN group in Capouet and Müller (2006) has been reduced in the current version of BOREAM. Uncertainty is very high, however, as vapour pressures for only one compound have been experimentally determined.

S1.2 Generic reactions

In the following tables, the reactions for one category of generic species are listed. The reaction rates and products are based on the reaction rates and product distributions for similar explicit compounds.

S1.2.1 Reactions of molecular generic species

Table S2: Reactions of generic molecular species: illustration for LX10e. R2R and RO3 are peroxy radical counters (see Capouet et al., 2004).

Reactants	Products	Reaction rate	Note
LX10eOOH + OH	→ LX10eCHO + OH	k_{seth}	a
LX10eOOH + OH	→ LX10kO2 + R2R	0.4 k_{LX}	g
	→ LX10iO3 + RO3	0.3 k_{LX}	h
	→ LX10eCHO + OH	0.3 k_{LX}	i
LX10eOH + OH	→ LX10eCHO + HO_2	k_{seth}	b
LX10eOH + OH	→ LX10iO2 + R2R	0.4 k_{LX}	g
	→ LX10gO3 + RO3	0.3 k_{LX}	h
	→ LX10cCHO + OH	0.3 k_{LX}	i
LX10eCHO + OH	→ LX10eO3 + RO3	k_{carb}	c
LX10eCHO + NO_3	→ LX10eO3 + RO3 + HNO_3	$k_{\mathrm{NO_3}}$	d
LX10eCHO + OH	→ LX10gO2 + R2R	0.4 k_{LX}	g
	→ LX10eO3 + RO3	0.3 k_{LX}	h
	→ LX10aCHO + OH	0.3 k_{LX}	i
LX10eCAR + OH	→ LX10gO3 + RO3	k_{carb}	c
LX10eCAR + NO_3	→ LX10gO3 + RO3 + HNO_3	$k_{\mathrm{NO_3}}$	d
LX10eCAR + OH	→ LX10iO2 + R2R	0.4 k_{LX}	g
	→ LX10gO3 + RO3	0.3 k_{LX}	h
	→ LX10cCHO + OH	0.3 k_{LX}	i
LX10eKET + OH	→ LX10gO2 + R2R	0.4 k_{LX}	g
	→ LX10eO3 + RO3	0.3 k_{LX}	h
	→ LX10aCHO + OH	0.3 k_{LX}	i
LX10ePAN + OH	→ LX10kO2 + R2R + NO_2	0.4 k_{LX}	g
	→ LX10iO3 + RO3 + NO_2	0.3 k_{LX}	h
	→ LX10eCHO + OH + NO_2	0.3 k_{LX}	i
LX10eONO2 + OH	→ LX10eCHO + NO_2	0.07 k_{seth}	e
LX10eONO2 + OH	→ LX10hO2 + R2R + NO_2	0.4 k_{LX}	g
	→ LX10fO3 + RO3 + NO_2	0.3 k_{LX}	h
	→ LX10bCHO + OH + NO_2	0.3 k_{LX}	i
LX10eCOOH + OH	→ LX9dO2 + R2R + CO_2	$k_{\mathrm{H-abst.ROH}}$	f,j
LX10eCOOH + OH	→ LX10kO2 + R2R	0.4 k_{LX}	g
	→ LX10iO3 + RO3	0.3 k_{LX}	h
	→ LX10eCHO + OH	0.3 k_{LX}	i
LX10eCOOOH + OH	→ LX10eO3 + H_2O + RO3	$k_{\mathrm{H-abst.ROOH}}$	f,j
LX10eCOOOH + OH	→ LX10kO2 + R2R	0.4 k_{LX}	g
	→ LX10iO3 + RO3	0.3 k_{LX}	h
	→ LX10eCHO + OH	0.3 k_{LX}	i

[a],[b] $k_{\mathrm{seth}} = 5.32 \times 10^{-12}\mathrm{cm^3molecule^{-1}s^{-1}}$, based on the rate recommended by Neeb (2000) for abstraction of a secondary H from the α-carbon, bearing an -OH or -OOH group. H-abstraction from oxygen atoms is ignored.
[c] H-abstraction from the -CHO group: $k_{\mathrm{carb}} = 16.9 \times 10^{-12}\mathrm{cm^3molecule^{-1}s^{-1}}$, based on measurements reported by Atkinson et al. (2006) and Schurath and Naumann (2003).
[d] $k_{\mathrm{NO_3}} = 1.67\ \exp(-1460/T)10^{-12}\mathrm{cm^3molecule^{-1}s^{-1}}$ (Atkinson et al., 2006).
[e] based on Neeb (2000).
[f] based on Neeb (2000), for abstraction of an H attached to a single oxygen ($k_{\mathrm{H-abst.ROH}} = 0.8 \times 10^{-12}\mathrm{cm^3molecule^{-1}s^{-1}}$) or to a peroxy group ($k_{\mathrm{H-abst.ROOH}} = 2.0 \times 10^{-12}\mathrm{cm^3molecule^{-1}s^{-1}}$).
[g] H-abstraction from an implicit aliphatic carbon, leading to a peroxy radical.
[h] H-abstraction from an implicit aldehydic carbon, leading to an acyl peroxy radical.
[i] H-abstraction from an implicit carbon bearing an α-hydroperoxide function, leading to a carbonyl and an OH radical.
[g] to [i] : For OH-reactions with the implicit part of the generic compound; $k_{\mathrm{LX}} = 8.0 \times 10^{-12}\mathrm{cm^3molecule^{-1}s^{-1}}$. The branching ratios of the reaction pathways described in notes [g] to [i] depend on the presence of functional groups in the parent structure, and therefore also on its vapour pressure (as vapour pressure and functionalisation are correlated). We assume these branching ratios have the values (0.6,0.2,0.2) for classes 'a' to 'c', (0.4,0.3,0.3) for classes 'd'-'g' and (0.2,0.4,0.4) for classes 'h'-'k'.

S1.2.2 Photolysis of molecular generic species

Table S3: Photolysis of molecular generic species: illustration for LX10e.

Reactants	Products	Reaction rate	Note
LX10eOOH + hν	$\rightarrow$ LX10eO + OH	2 · j(LXCH3OOH)	a,b
LX10eOOH + hν	$\rightarrow$ LX8aOOH + CH3CHO	j(LXALD)	c
LX10eOH + hν	$\rightarrow$ LX10cO + OH	j(LXCH3OOH)	b
LX10eOH + hν	$\rightarrow$ LX8aOH + CH3CHO	j(LXALD)	c
LX10eCHO + hν	$\rightarrow$ LX8cO2 + R2R + CH3CHO	0.8 · j(ALD)	a,d
	$\rightarrow$ LX9dO2 + R2R + CO	0.2 · j(ALD)	
LX10eCHO + hν	$\rightarrow$ LX10aO + OH	j(LXCH3OOH)	b
LX10eCHO + hν	$\rightarrow$ LX8aCHO + CH3CHO	j(LXALD)	c
LX10eCAR + hν	$\rightarrow$ LX8eKET + CH3CHO	0.8 · j(ALD)	a
	$\rightarrow$ LX9fO2 + R2R + CO	0.2 · j(ALD)	
LX10eCAR + hν	$\rightarrow$ LX7dKET + CH3CHO	0.8 · j(keto)	
	$\rightarrow$ LX8eO2 + R2R + CH3CO	0.2 · j(keto)	
LX10eCAR + hν	$\rightarrow$ LX10cO + OH	j(LXCH3OOH)	b
LX10eCAR + hν	$\rightarrow$ LX8aCOOOH + CH3CHO	j(LXALD)	c
LX10eKET + hν	$\rightarrow$ LX8cO2 + R2R + CH3CHO	0.8 · j(keto)	a,d
LX10eKET + hν	$\rightarrow$ LX8cO2 + R2R + CH3CO3 + RO3	0.2 · j(keto)	
LX10eKET + hν	$\rightarrow$ LX10aO + OH	j(LXCH3OOH)	b
LX10eKET + hν	$\rightarrow$ LX8aKET + CH3CHO	j(LXALD)	c
LX10ePAN + hν	$\rightarrow$ LX10eO3 + NO2 + RO3	0.8 · j(ppn)	a
LX10ePAN + hν	$\rightarrow$ LX10eO2 + NO3 + R2R	0.2 · j(ppn)	
LX10ePAN	$\rightarrow$ LX10eO3 + NO2 + RO3	k_{PAN}	a
LX10ePAN + hν	$\rightarrow$ LX10eO + OH + NO2	j(LXCH3OOH)	b
LX10ePAN + hν	$\rightarrow$ LX8aPAN + CH3CHO	j(LXALD)	c
LX10eONO2 + hν	$\rightarrow$ LX10eO + NO2	j(nitu)	a
LX10eONO2 + hν	$\rightarrow$ LX10aO + OH + NO2	j(LXCH3OOH)	b
LX10eONO2 + hν	$\rightarrow$ LX8bONO2 + CH3CHO	j(LXALD)	c
LX10eCOOH + hν	$\rightarrow$ LX10eO + OH	j(LXCH3OOH)	b
LX10eCOOH + hν	$\rightarrow$ LX8aCOOH + CH3CHO	j(LXALD)	c
LX10eCOOOH + hν	$\rightarrow$ LX9dO2 + R2R + CO2 + OH	j(peracid)	a
LX10eCOOOH + hν	$\rightarrow$ LX10eO + OH	j(LXCH3OOH)	b
LX10eCOOOH + hν	$\rightarrow$ LX8aCOOOH + CH3CHO	j(LXALD)	c

[a] The J-values for photolysis of the explicitly represented groups and the product distributions follow Capouet et al. (2004) and Capouet et al. (2008).

[b],[c] Photolysis of the implicit part of the molecule, assumed to proceed as for a compound containing one hydroperoxide group (b) and one aldehyde group (c). For classes 'a' to 'd', the J-values are halved, due to expected lower functionalisation.

[b] Photolysis of a hydroperoxide group in the implicit part of the compound, resulting in an alkoxy radical and OH.

[c] Aldehyde photolysis in the implicit part is assumed to follow the Norrish-type II reaction, which leads to an alkene and ethaldehyde (see Paulson et al., 2006). This results in removal of 2 carbons and the aldehyde group from the implicit part of the generic species, increasing volatility (here from class 'e' to 'a').

[d] For explicit aldehyde and ketone photolysis, branching ratios of 0.8 for Norrish-type II reaction (leading to an alkene and ethaldehyde), and 0.2 for the radical channel are assumed. In the first case, the alkene is then assumed to quickly react with OH or ozone, yielding a peroxy radical.

S1.2.3 Generic alkoxy radical reactions

Table S4: Reactions of generic alkoxy radicals: illustration with the radical LX10eO.

Reactants	Products	Branching ratios	Note
LX10eO + O_2	→ LX10eCHO + HO_2	0.15	a,g
LX10eO	→ LX9dO2 + R2R + CH_2O	0.3	b,f,g
	→ LX9bO3 + RO3 + CH_2O	0.1	f
	→ LX9aCHO + OH + CH_2O	0.1	f
LX10eO	→ LX9aO2 + R2R + HCOOH	0.05	c,g
LX10eO	→ LX7aO2 + R2R + acetone	0.10	d,g
LX10eO	→ LX10iO2 + R2R	0.12	e,f,g
	→ LX10gO3 + RO3	0.04	f
	→ LX10cCHO + OH	0.04	f

[a] Assumed branching ratio for reaction with O_2.
[b] We consider three types of decomposition, with the most common being of the type RCH2O· → R· + CH_2O.
[c] This decomposition follows RCH(OH)O· → R· + HCOOH .
[d] This decomposition reaction follows R(CH3CO·CH3) → R· + acetone .
[e] H-shift isomerisation, as in RCH2CH2CH2CH2O· → RC·HCH2CH2CH2OH .
[f] An alkyl radical is produced. Alkyl radicals without an α-functionality react with O_2, forming peroxy radicals. However, alkyl radicals bearing an α-aldehyde function generate acyl alkoxy radicals, and in case of a possible α-hydroperoxide, the radical becomes an aldehyde + OH. The assumed branching ratios for these three possible pathways are $(0.6, 0.2, 0.2)$ for classes 'e' to 'k' and $(0.8, 0.1, 0.1)$ for classes 'a' to 'd'.
[g] The branching ratios depend on the vapour pressure class (see Table S5).

Table S5: Branching ratios for generic alkoxy radicals depending on their vapour pressure class.

Alkoxy radical reaction pathway	class a-c	class d-g	class h-k
reaction with O_2	0.20	0.15	0.05
CH_2O elimination	0.40	0.5	0.65
HCOOH elimination	0.05	0.05	0.05
acetone elimination	0.05	0.10	0.15
H-shift isomerisation	0.30	0.2	0.10

Decomposition is more likely for the more chemically functionalised species (see for example Vereecken and Peeters, 2009). Therefore, the assumed branching ratios for decomposition increase with decreasing vapour pressure, since we assume an inverse correlation between number of functional groups present and vapour pressure.

S1.2.4 Generic peroxy radical reactions

Table S6: Reactions of generic peroxy radicals: illustration with radical LX10eO2.

Reactants	Products	Reaction rate	Note
LX10eO2 + NO	→ LX10eO + NO2 - R2R	$0.9 \cdot k_{\mathrm{NO,RO_2}}$	a,b
LX10eO2 + NO	→ LX10eONO2 - R2R	$0.1 \cdot k_{\mathrm{NO,RO_2}}$	a,b
LX10eO2 + NO3	→ LX10eO + NO2 - R2R	$k_{\mathrm{NO_3,RO_2}}$	a,c
LX10eO2 + HO2	→ LX10eOOH - R2R	$k_{\mathrm{HO_2,RO_2}}$	a,d
LX10eO2 + R3R	→ 0.70 LX10eO + 0.30 LX10eCHO	$k_{\mathrm{R2R,R3R}}$	a
LX10eO2 + R3O	→ 0.70 LX10eO + 0.30 LX10eCHO	$k_{\mathrm{R2R,R3O}}$	a
LX10eO2 + R3H	→ 0.70 LX10eO + 0.30 LX10eCHO	$k_{\mathrm{R2R,R3H}}$	a
LX10eO2 + R2R	→ 0.50 LX10eO + 0.25 LX10eCHO + 0.25 LX10eOH	$k_{\mathrm{R2R,R2R}}$	a
LX10eO2 + R2O	→ 0.50 LX10eO + 0.25 LX10eCHO + 0.25 LX10eOH	$k_{\mathrm{R2R,R3R}}$	a
LX10eO2 + R2H	→ 0.50 LX10eO + 0.25 LX10eCHO + 0.25 LX10eOH	$k_{\mathrm{R2R,R2H}}$	a
LX10eO2 + R1R	→ 0.50 LX10eO + 0.25 LX10eCHO + 0.25 LX10eOH	$k_{\mathrm{R2R,R1R}}$	a
LX10eO2 + R1H	→ 0.50 LX10eO + 0.25 LX10eCHO + 0.25 LX10eOH	$k_{\mathrm{R2R,R1H}}$	a
LX10eO2 + RO3	→ LX10eO	$r_{\mathrm{oxyr}} \cdot k_{\mathrm{RO_2,RO_3}}$	a,e,f
LX10eO2 + RO3	→ LX10eCHO	$r_{\mathrm{acid}} \cdot k_{\mathrm{RO_2,RO_3}}$	a,e,f

[a] Peroxy radicals are grouped into 9 classes according to their functionality, and their cross reactions are then treated using a system of peroxy radical class counters (Capouet et al., 2004). Generic peroxy radicals are assumed to behave as the so-called R2R-class, which contains secondary peroxy radicals without α- or β-functional groups. The cross-reaction rates $k_{\mathrm{R2R,R3R}}$, etc., can be calculated using Table 2 and Eq. 3 in Capouet et al. (2004), and the product distributions follow Table 1 in Capouet et al. (2004).

[b] $k_{\mathrm{NO,RO_2}} = 2.54 \times 10^{-12} \exp(360/T)$ cm^3 molecule^{-1}s^{-1} (Saunders et al., 2003). The estimated alkyl nitrate yield is 0.1 (see Capouet et al. (2004))).

[c] $k_{\mathrm{NO_3,RO_2}} = 2.3 \times 10^{-12}$ cm^3 molecule^{-1}s^{-1}(based on $C_2H_5O_2$ in Atkinson et al. (2006)).

[d] $k_{\mathrm{HO_2,RO_2}} = 2.72 \times 10^{-13} \exp(1250/T)$ cm^3 molecule^{-1}s^{-1} (Saunders et al., 2003).

[e] For the cross-reactions between peroxy radicals and acyl peroxy radicals the rate constant $k_{\mathrm{RO_2,RO_3}} = 1.0{\times}10^{-11}$ cm^3 molecule^{-1}s^{-1} is used (Capouet et al., 2004).

[f] The branching ratios of the alkoxy radical channel and the molecular channel are given by $r_{\mathrm{acid}} = 1/(1 + 2.2 \cdot 10^6 \exp(-3280/T))$ and $r_{\mathrm{oxyr}} = 1 - r_{\mathrm{acid}}$.

S1.2.5 Generic acyl peroxy radical reactions

Table S7: Reactions of generic acyl peroxy radicals: illustration with radical LX10eO3.

Reactants	Products	Reaction rate	Note
LX10eO3 + NO	→ CO_2 + 0.60 LX9dO2 + 0.60 R2R + 0.20 LX9bO3 + 0.20 RO3 + 0.20 LX9aCHO + 0.20 OH + NO2 - RO3	k_{NO,RO_3}	a,g
LX10eO3 + NO2	→ LX10ePAN - RO3	k_{NO_2,RO_3}	b
LX10eO3 + NO3	→ CO_2 + 0.60 LX9dO2 + 0.60 R2R + 0.20 LX9bO3 + 0.20 RO3 + 0.20 LX9aCHO + 0.20 OH + NO2 - RO3	k_{NO_3,RO_3}	c,g
LX10eO3 + HO2	→ LX10eCOOH + O3 - RO3	$0.13 \cdot k_{HO_2,RO_3}$	d
LX10eO3 + HO2	→ LX10eCOOOH + O2 - RO3	$0.41 \cdot k_{HO_2,RO_3}$	d
LX10eO3 + HO2	→ CO_2 + 0.60 LX9dO2 + 0.60 R2R + 0.20 LX9bO3 + 0.20 RO3 + 0.20 LX9aCHO + 0.20 OH + OH - RO3	$0.46 \cdot k_{HO_2,RO_3}$	d,g
LX10eO3 + R3R	→ CO_2 + 0.60 LX9dO2 + 0.60 R2R + 0.20 LX9bO3 + 0.20 RO3 + 0.20 LX9aCHO + 0.20 OH	k_{RO_2,RO_3}	e,g
LX10eO3 + R3O	→ CO_2 + 0.60 LX9dO2 + 0.60 R2R + 0.20 LX9bO3 + 0.20 RO3 + 0.20 LX9aCHO + 0.20 OH	k_{RO_2,RO_3}	g
LX10eO3 + R3H	→ CO_2 + 0.60 LX9dO2 + 0.60 R2R + 0.20 LX9bO3 + 0.20 RO3 + 0.20 LX9aCHO + 0.20 OH	k_{RO_2,RO_3}	g
LX10eO3 + R2R	→ CO_2 + 0.60 LX9dO2 + 0.60 R2R + 0.20 LX9bO3 + 0.20 RO3 + 0.20 LX9aCHO + 0.20 OH	$r_{oxyr} \cdot k_{RO_2,RO_3}$	g
LX10eO3 + R2R	→ LX10eCOOH	$r_{acid} \cdot k_{RO_2,RO_3}$	
LX10eO3 + R2O	→ CO_2 + 0.60 LX9dO2 + 0.60 R2R + 0.20 LX9bO3 + 0.20 RO3 + 0.20 LX9aCHO + 0.20 OH	$r_{oxyr} \cdot k_{RO_2,RO_3}$	g
LX10eO3 + R2O	→ LX10eCOOH	$r_{acid} \cdot k_{RO_2,RO_3}$	
LX10eO3 + R2H	→ CO_2 + 0.60 LX9dO2 + 0.60 R2R + 0.20 LX9bO3 + 0.20 RO3 + 0.20 LX9aCHO + 0.20 OH	$r_{oxyr} \cdot k_{RO_2,RO_3}$	g
LX10eO3 + R2H	→ LX10eCOOH	$r_{acid} \cdot k_{RO_2,RO_3}$	
LX10eO3 + R1R	→ CO_2 + 0.60 LX9dO2 + 0.60 R2R + 0.20 LX9bO3 + 0.20 RO3 + 0.20 LX9aCHO + 0.20 OH	$r_{oxyr} \cdot k_{RO_2,RO_3}$	g
LX10eO3 + R1R	→ LX10eCOOH	$r_{acid} \cdot k_{RO_2,RO_3}$	
LX10eO3 + R1O	→ CO_2 + 0.60 LX9dO2 + 0.60 R2R + 0.20 LX9bO3 + 0.20 RO3 + 0.20 LX9aCHO + 0.20 OH	$r_{oxyr} \cdot k_{RO_2,RO_3}$	g
LX10eO3 + R1O	→ LX10eCOOH	$r_{acid} \cdot k_{RO_2,RO_3}$	
LX10eO3 + R1H	→ CO_2 + 0.60 LX9dO2 + 0.60 R2R + 0.20 LX9bO3 + 0.20 RO3 + 0.20 LX9aCHO + 0.20 OH	$r_{oxyr} \cdot k_{RO_2,RO_3}$	g
LX10eO3 + R1H	→ LX10eCOOH	$r_{acid} \cdot k_{RO_2,RO_3}$	
LX10eO3 + RO3	→ CO_2 + 0.60 LX9dO2 + 0.60 R2R + 0.20 LX9bO3 + 0.20 RO3 + 0.20 LX9aCHO + 0.20 OH	k_{self,RO_3}	f

[a] $k_{NO,RO_3} = 6.7 \times 10^{-12} \exp(340/T)$ cm^3 molecule^{-1}s^{-1}, based on $C_2H_5CO(O_2)$ (Atkinson et al., 2006).
[b] k_{NO_2,RO_3} is calculated using the high-pressure limit of the Troe-expression for the $CH_3C(O)O_2 + NO_2$ reaction (see Capouet et al. (2004) and references therein), which in this case is $1.2 \cdot 10^{-11}(T/300)^{-0.9}$ cm^3 molecule^{-1}s^{-1} (Atkinson et al., 2006).
[c] $k_{NO_3,RO_3} = 4.3 \times 10^{-12}$ cm^3 molecule^{-1}s^{-1} based on $CH_3CO(O_2)$(Saunders et al., 2003).
[d] The product distribution is based on $CH_3C(O)O_2 + HO_2$ Jenkin et al. (2007). The reaction rate $k_{HO_2,RO_3} = 5.2 \times 10^{-13} \exp(983/T)$ cm^3 molecule^{-1}s^{-1} is used (see Capouet et al. (2004)).
[e] For the cross-reactions between peroxy radicals and acyl peroxy radicals the rate constant $k_{RO_2,RO_3} = 1.0 \times 10^{-11}$ cm^3 molecule^{-1}s^{-1} is used (Capouet et al., 2004).
[f] For the self-reactions of acyl peroxy radicals, $k_{self,RO_3} = 1.5 \times 10^{-11}$ cm^3 molecule^{-1}s^{-1} is used (Capouet et al., 2004).
[g] In these reactions an acyl alkoxy radical is produced, which decomposes into an alkyl radical and CO_2. Treatment of alkyl radicals follows note f in Table S4 .

S2 BOREAM Model validation

We present a comparison of measured time series for α-pinene, ozone, NO_x and SOA with simulations performed with the full BOREAM model. First we show simulations for a low-NO_x experiment (1) and a high-NO_x experiment (4) from Ng et al. (2007). The time series and discussion of some aspects concerning the simulations are given in Valorso et al. (2011). Initial concentrations for important species for which measurements were not available were optimised in order to obtain good agreement for observed α-pinene decay. For three experiments from Carter (2000) we compare the quantity $D(O_3 - NO) = ([O_3] - [O_3]_{initial}) - ([NO] - [NO]_{initial})$, which is an indication for the strength of ozone production.

Table S8: Initial settings for concentrations of VOC and inorganic compounds in the experiments 1 and 4 from Ng et al. (2007), discussed in Valorso et al. (2011). Optimised initial values and wall sources differ slightly from those in Valorso et al. (2011)

Initial settings	Exp. 1	Exp. 4
available measurements		
temperature	298 K	299 K
Relative humidity	5.3%	3.3%
[α-pinene]	13.8 ppb	12.6 ppb
[O_3]	4 ppb	not available
[NO]	not available	475 ppb
[NO_2]	not available	463 ppb
model settings for unmeasured parameters		
[O_3]	measured value	0 ppb
[NO]	0.35 ppb	measured value
[NO_2]	0.35 ppb	measured value
[H_2O_2]	1250 ppb	0 ppb
[HONO]	0 ppb	1000 ppb
$J(NO_2)$	$3.3 \cdot 10^{-1}$min^{-1}	$4.2 \cdot 10^{-1}$min^{-1}
$J(H_2O_2)$	$1.35 \cdot 10^{-4}$min^{-1}	$1.7 \cdot 10^{-4}$min^{-1}
NO wall source	0.5 ppt min^{-1}	none
NO_2 wall source	0.5 ppt min^{-1}	none
unknown OH source	none	$1.8 \cdot 10^{9}$molec cm^{3}s^{-1}
aerosol wall loss	$1.\cdot 10^{-5}$ s^{-1}	$1. \cdot 10^{-5}$s^{-1}

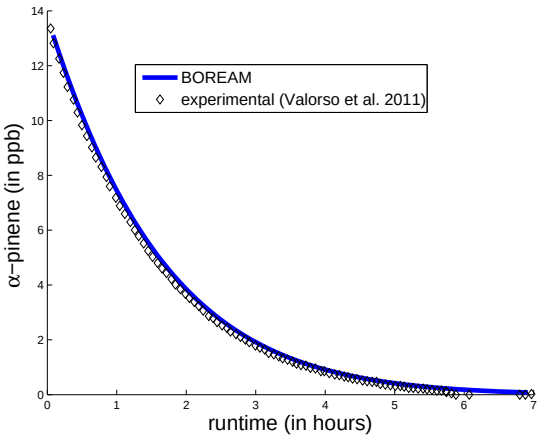

Figure S1: Measured and full BOREAM model α-pinene concentrations for experiment 1 of Ng et al. (2007).

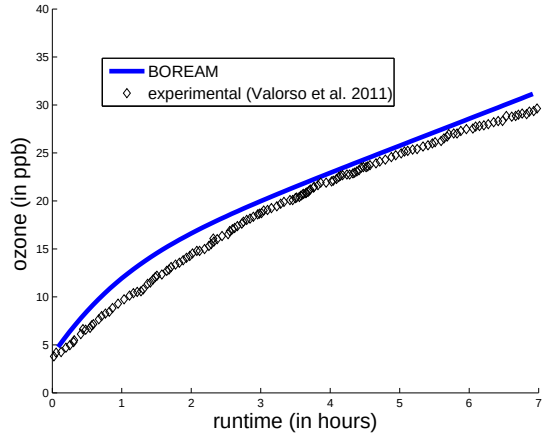

Figure S2: Measured and full BOREAM model ozone concentrations for experiment 1 of Ng et al. (2007).

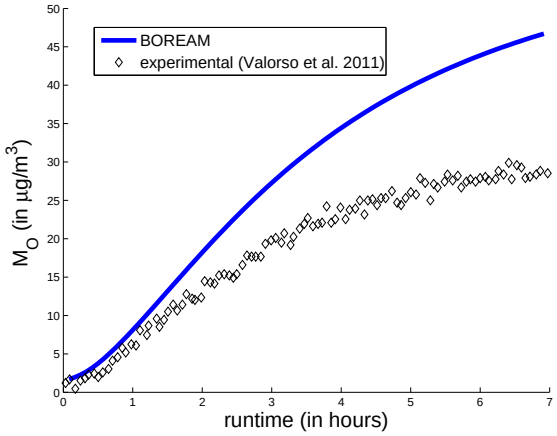

Figure S3: Measured and full BOREAM model SOA mass concentrations for experiment 1 of Ng et al. (2007).

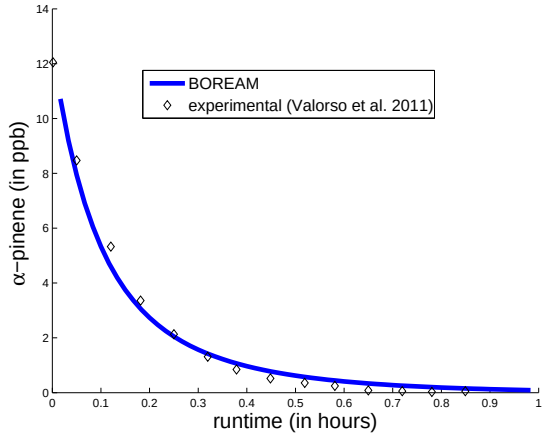

Figure S4: Measured and full BOREAM model α-pinene concentrations for experiment 4 of Ng et al. (2007).

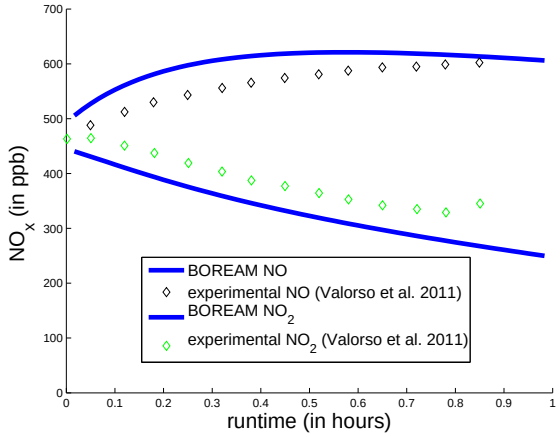

Figure S5: Measured and full BOREAM model NO and NO_2 concentrations for experiment 4 of Ng et al. (2007).

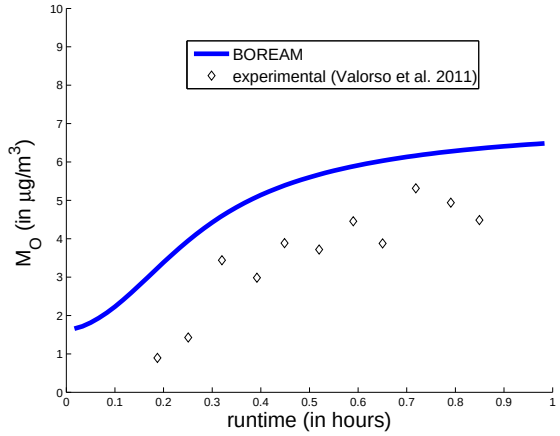

Figure S6: Measured and full BOREAM model SOA mass concentrations for experiment 4 of Ng et al. (2007).

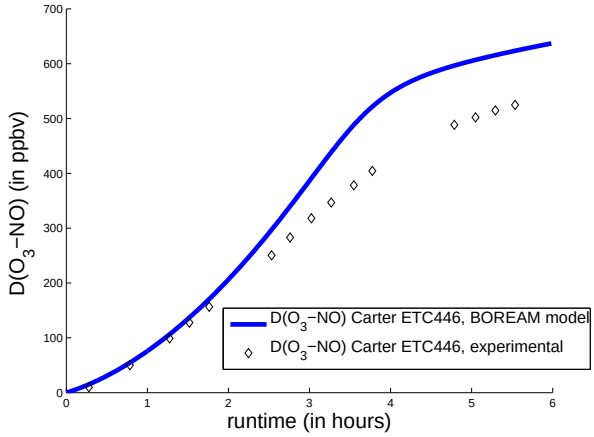

Figure S7: Measured and full BOREAM model $D(\mathrm{O_3}-\mathrm{NO})$ (in ppb) for experiment ETC446 of Carter (2000).

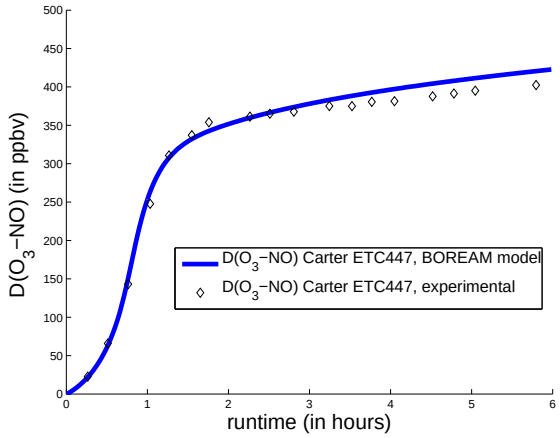

Figure S8: Measured and full BOREAM model $D(\mathrm{O_3}-\mathrm{NO})$ (in ppb) for experiment ETC447 of Carter (2000).

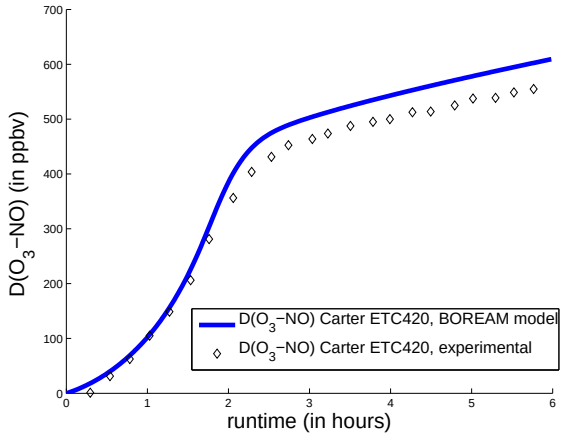

Figure S9: Measured and full BOREAM model $D(\mathrm{O_3}-\mathrm{NO})$ (in ppb) for experiment ETC420 of Carter (2000).

S3 Fitting procedure for the photochemical SOA loss

For each oxidation scenario and each temperature, the sensitivity calculations illustrated in Figs. 3a and 3b in Sect. 3.2 of the main article were used to estimate the amount of organic aerosol lost due to photochemical processing at SOA equilibrium, $[\mathrm{OA}]_{\mathrm{pl}}$, for the simulation at an α-pinene concentration which leads to an SOA concentration of around 2.5 $\mu\mathrm{gm}^{-3}$. The maximum (noontime) photochemical loss rate is fitted to reproduce the condensable material lost during one day at SOA equilibrium. We use the formula
$[\mathrm{OA}]_{\mathrm{pl}} = \int_{\mathrm{day13}} J_{\mathrm{pl,max}} \cdot S(t) \cdot [\mathrm{OA}](t)dt$ (4.1),
where $S(t)$ denotes the diurnal shape factor (between 0 and 1) adopted for all photolysis rates in the box model calculations. For the NO_3–oxidation scenario at high temperatures, it turns out that the estimated values of $[\mathrm{OA}]_{\mathrm{pl}}$ are too large. Therefore in such cases, a correction was applied. At α-pinene concentrations differing from those of the above fitting , we then insert the derived $J_{\mathrm{pl,max}}$ in formula 4.1, which together with the simulated SOA concentration $[OA](t)$ allows us to deduce the value of $[\mathrm{OA}]_{\mathrm{pl}}$ for that α-pinene concentration. This $[\mathrm{OA}]_{\mathrm{pl}}$ is then used to calculate the SOA yield according to formula $([\mathrm{OA}]_{\mathrm{dep.}}+[\mathrm{OA}]_{\mathrm{pl}})/\Delta[\alpha\text{-pinene}]$.

The retrieved yield parameters and SOA photolysis rates are inserted in the parameter model, which is then used to simulate the 5 oxidation scenarios at varying temperatures and α-pinene concentrations. At this stage a final optimization of $J_{\mathrm{pl,max}}$ is performed in order to improve the agreement of the time evolution of M_O between full and parameter model in the range of atmospherically relevant M_O concentrations. We then perform a fitting of $J_{\mathrm{pl,max}}$ as a function of temperature for each of the 5 scenarios. From these maximum photolysis rates, the J-values J_{pl} for the photochemical loss rates can be obtained as explained in the

main article. The parameters for the polynomial fittings for the factors $f_{\mathrm{pl,max}}$ are given and graphically represented below for each of the five oxidation scenarios.

Table S9: Polynomial coefficients for the temperature dependent fitting $f_{\mathrm{pl,max}} = \sum_{i=0}^{5} a_i (T - 273)^i$.

Scenario	a_5	a_4	a_3	a_2	a_1	a_0
low-NO_x, OH	$-4.146 \cdot 10^{-8}$	$1.959 \cdot 10^{-6}$	$-1.962 \cdot 10^{-5}$	$-7.746 \cdot 10^{-5}$	$1.483 \cdot 10^{-3}$	$7.292 \cdot 10^{-2}$
high-NO_x, OH	$3.316 \cdot 10^{-7}$	$-2.291 \cdot 10^{-5}$	$5.544 \cdot 10^{-4}$	$-4.917 \cdot 10^{-3}$	$1.555 \cdot 10^{-2}$	$2.268 \cdot 10^{-1}$
low-NO_x, O_3	$6.577 \cdot 10^{-8}$	$-5.243 \cdot 10^{-6}$	$1.4078 \cdot 10^{-4}$	$-1.375 \cdot 10^{-3}$	$2.452 \cdot 10^{-3}$	$1.293 \cdot 10^{-1}$
high-NO_x, O_3	$-2.646 \cdot 10^{-7}$	$2.116 \cdot 10^{-5}$	$-6.161 \cdot 10^{-4}$	$8.637 \cdot 10^{-3}$	$-4.354 \cdot 10^{-2}$	$3.187 \cdot 10^{-1}$
high-NO_x, NO_3	$3.536 \cdot 10^{-8}$	$-2.732 \cdot 10^{-6}$	$5.830 \cdot 10^{-5}$	$2.975 \cdot 10^{-4}$	$-1.902 \cdot 10^{-2}$	$1.649 \cdot 10^{-1}$

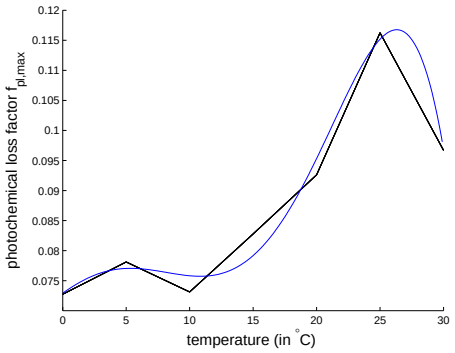

Figure S10: Temperature dependent fit (in blue) in the low-NO_x OH oxidation case for the photochemical loss factor $f_{\mathrm{pl,max}}$, which allows calculation of the J-value for the photochemical loss reaction in the parameter model through $J_{\mathrm{pl}} = f_{\mathrm{pl,max}} \cdot J_{\mathrm{ald}}$.

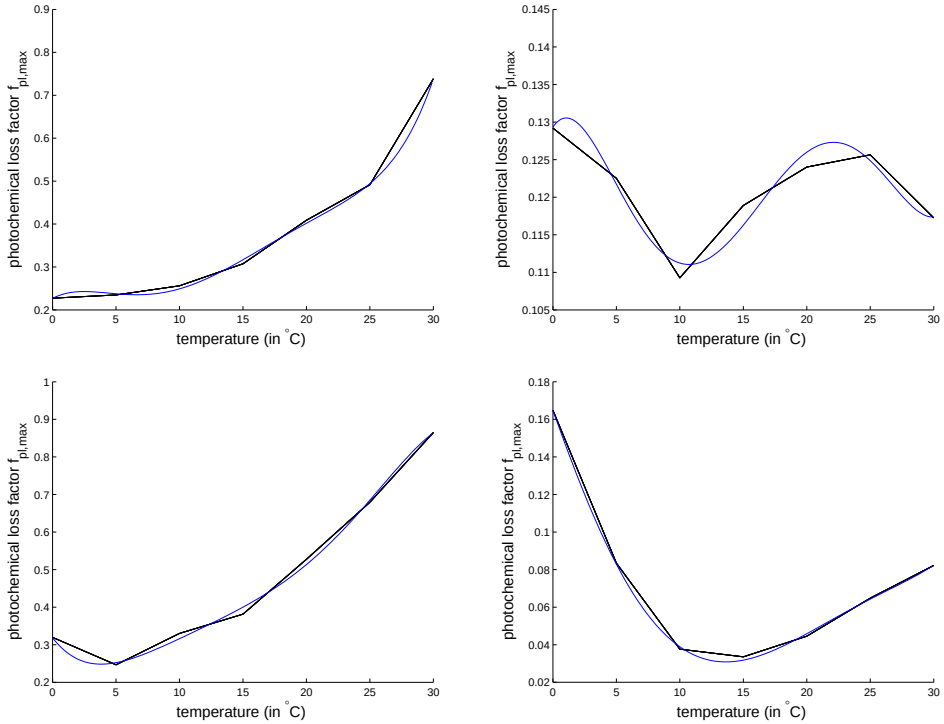

Figure S11: $f_{\mathrm{pl,max}}$ (in blue) for the high-NO_x OH oxidation (upper left), low-NO_x O_3 oxidation (upper right), high-NO_x O_3 oxidation (lower left), and high-NO_x NO_3 oxidation (lower right).

S4 SOA parameterisation agreement with full model

In the following Table we evaluate the level of agreement between the full and the parameter model for the 5 oxidation scenarios, which were simulated at 7 temperatures and at a number of different α-pinene concentrations. In each simulation SOA build-up was simulated over 14 day. Simulations for which the maximum M_O reached did not fall in the range 0.5–20 μgm^{-3} were not considered. The following table provides the percentage of simulated days satisfying a given level of agreement, using a deviation factor defined as $\exp(|\log(\overline{M_{O,p}}/\overline{M_{O,f}})|)$.

Table S10: Percentage of days for which the model deviation factor falls within the range 1 to 1.25 (first part), or exceeds a factor 2 (second part).

Scenario	273 K	278 K	283 K	288 K	293 K	298 K	303 K
low-NO_x, OH	98.2	97.3	94.6	91.7	85.7	84.5	81.2
high-NO_x, OH	95.5	95.0	93.5	87.9	80.1	89.3	78.6
low-NO_x, O_3	98.2	98.2	97.6	91.1	83.3	76.8	80.4
high-NO_x, O_3	92.9	83.6	94.4	92.1	88.9	85.7	57.1
high-NO_x, NO_3	86.7	80.4	73.5	70.4	64.3	68.4	53.1
low-NO_x, OH	0	0	0	0	0	1.8	5.8
high-NO_x, OH	0	0	0.6	2.9	5.6	5.4	16.3
low-NO_x, O_3	0	0	0	0	0	1.2	3.6
high-NO_x, O_3	2.1	2.1	0	0.8	3.2	6.1	7.1
high-NO_x, NO_3	3.1	2.7	2.0	1.0	5.1	11.2	27.6

Fig. S12 compares the full and parameterised model yields at various NO_x-levels for the ozonolysis scenario. Figs. S13 to S16 compare the full and parameter model for SOA formed under OH-oxidation at intermediate-NO_x and at temperatures between 273 K and 303 K.

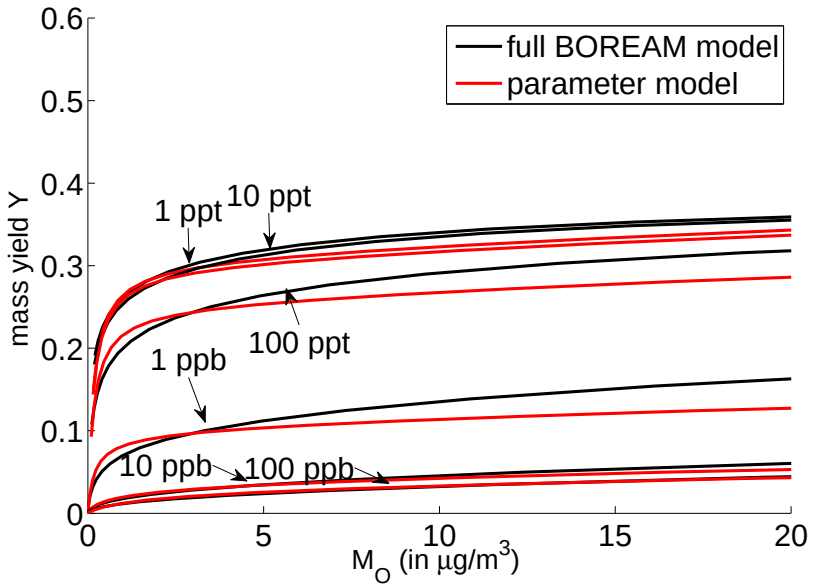

Figure S12: Net SOA yields near SOA equilibrium calculated by the full (black) and parameterised (red) model at various NO_2 levels, for ozone oxidation (at 298 K).

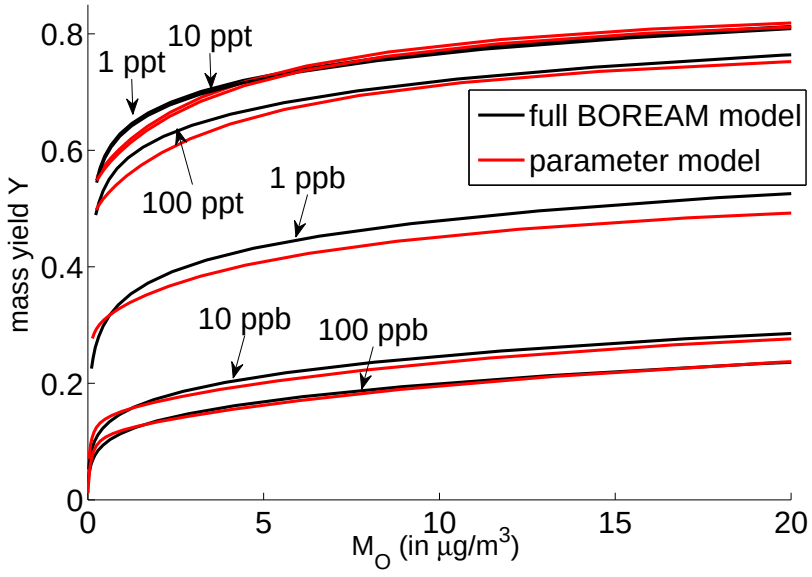

Figure S13: Comparison of full model (black) and parameter model (red) net SOA mass yields near SOA equilibrium in function of M_O for OH-oxidation, at 7 different NO_2 concentrations (at 273 K).

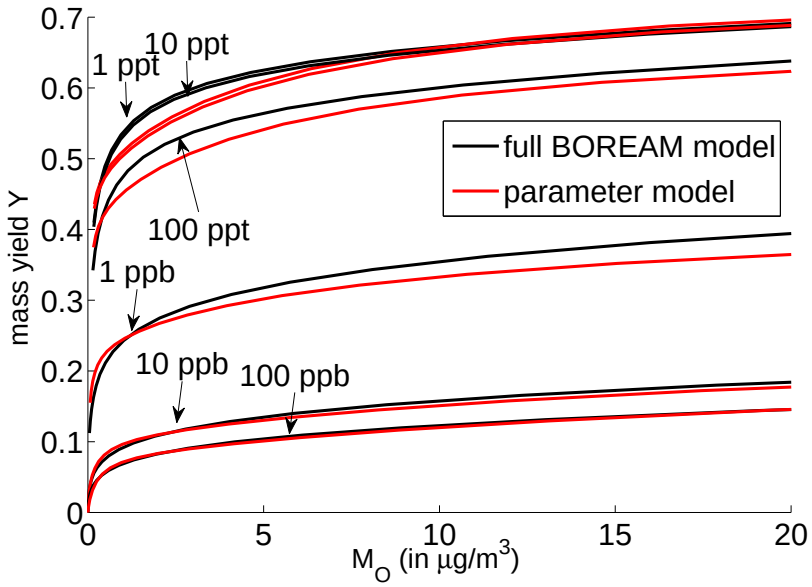

Figure S14: Comparison of full model (black) and parameter model (red) net SOA mass yields near SOA equilibrium in function of M_O for OH-oxidation, at 7 different NO_2 concentrations (at 283 K).

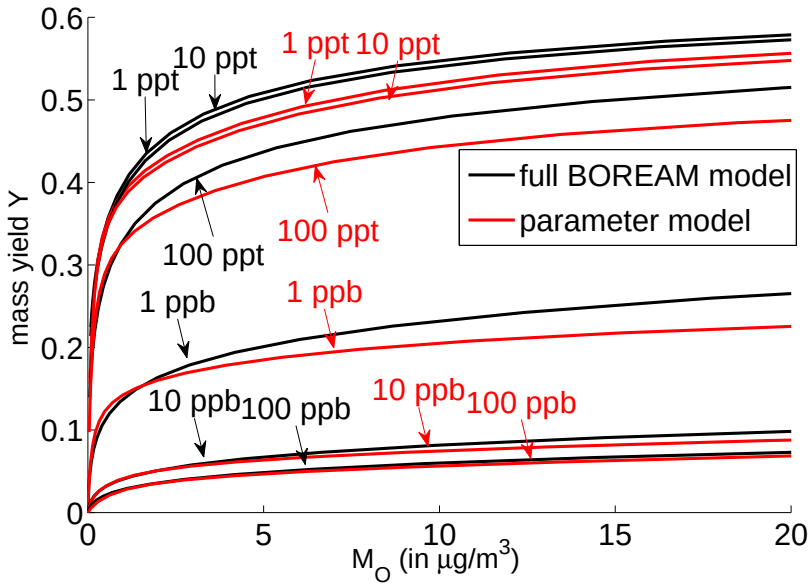

Figure S15: Comparison of full model (black) and parameter model (red) net SOA mass yields near SOA equilibrium in function of M_O for OH-oxidation, at 7 different NO_2 concentrations (at 293 K).

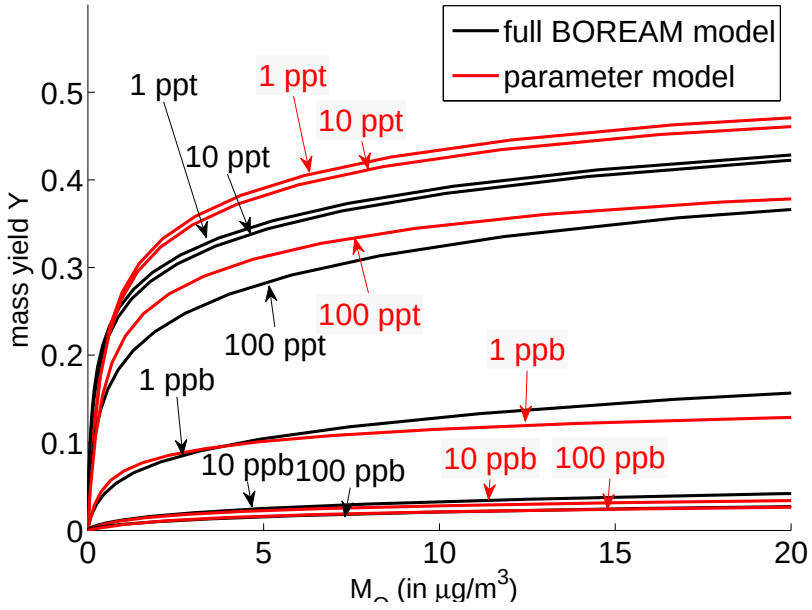

Figure S16: Comparison of full model (black) and parameter model (red) net SOA mass yields near SOA equilibrium in function of M_O for OH-oxidation, at 7 different NO_2 concentrations (at 303 K).

S5 Full BOREAM and parameter model for ambient conditions based on IMAGESv2

Table S11 provides an overview of the conditions and model results for the 17 locations considered, during the months of May until September. Fig. S17 displays the temporal dependence of the modelled α-pinene SOA concentrations in the parameter model and the full BOREAM model, for the month of July, at the locations for which these plots are not shown in the main article.

Table S11: Average temperature ($\overline{T}$), NO_x concentration ($\overline{[NO_x]}$), concentration of organic aerosol excluding $\alpha-$pinene SOA ($\overline{[OA_{other}]}$), concentration of α-pinene SOA calculated using BOREAM ($\overline{M_{O,f}}$) in the simulations based on IMAGESv2 output. The values are tropospheric averages weighted by the α-pinene oxidation product concentrations in the gas phase. The last two columns provide the averaged deviation and bias, expressed relatively to the average concentration in the full model simulation (see Sect.3.4.5 in the main article for the used formulas).

Location	$\overline{T}$ (in K)	$\overline{[NO_x]}$ (in ppt)	$\overline{[OA_{other}]}$ (in μgm^{-3})	$\overline{M_{O,f}}$ α-pinene (in $\mu g\ m^{-3}$)	averaged deviation	averaged bias
Surinam	278.7	53	1.2	1.70	0.16	0.15
South-East US	283.1	381	3.0	1.43	0.098	-0.036
Russia	269.8	142	0.65	0.64	0.093	-0.024
North-West US	271.8	390	0.81	0.37	0.12	-0.026
Mexico	278.	301	1.85	0.45	0.086	0.037
Peru	275.8	48	1.41	1.07	0.071	0.068
South-Brazil	265.9	122	0.68	0.11	0.16	0.011
Benin	278.4	185	2.02	0.77	0.067	-0.044
Congo	279.8	119	4.0	1.54	0.044	0.002
Belgium	267.1	648	0.77	0.084	0.092	0.018
Finland	271.3	323	0.75	0.44	0.18	-0.18
Pearl River Delta	274.0	752	2.07	0.79	0.19	-0.19
Beijing	278.6	723	1.56	0.26	0.084	-0.049
India, coastal	278.6	156	1.67	0.008	0.11	-0.037
Siberia	266.7	84	1.57	0.62	0.12	0.11
Borneo	280.0	127	2.14	1.00	0.11	0.10
Queensland	268.4	98	0.52	0.26	0.24	0.24
Overall				0.68	0.11	0.021

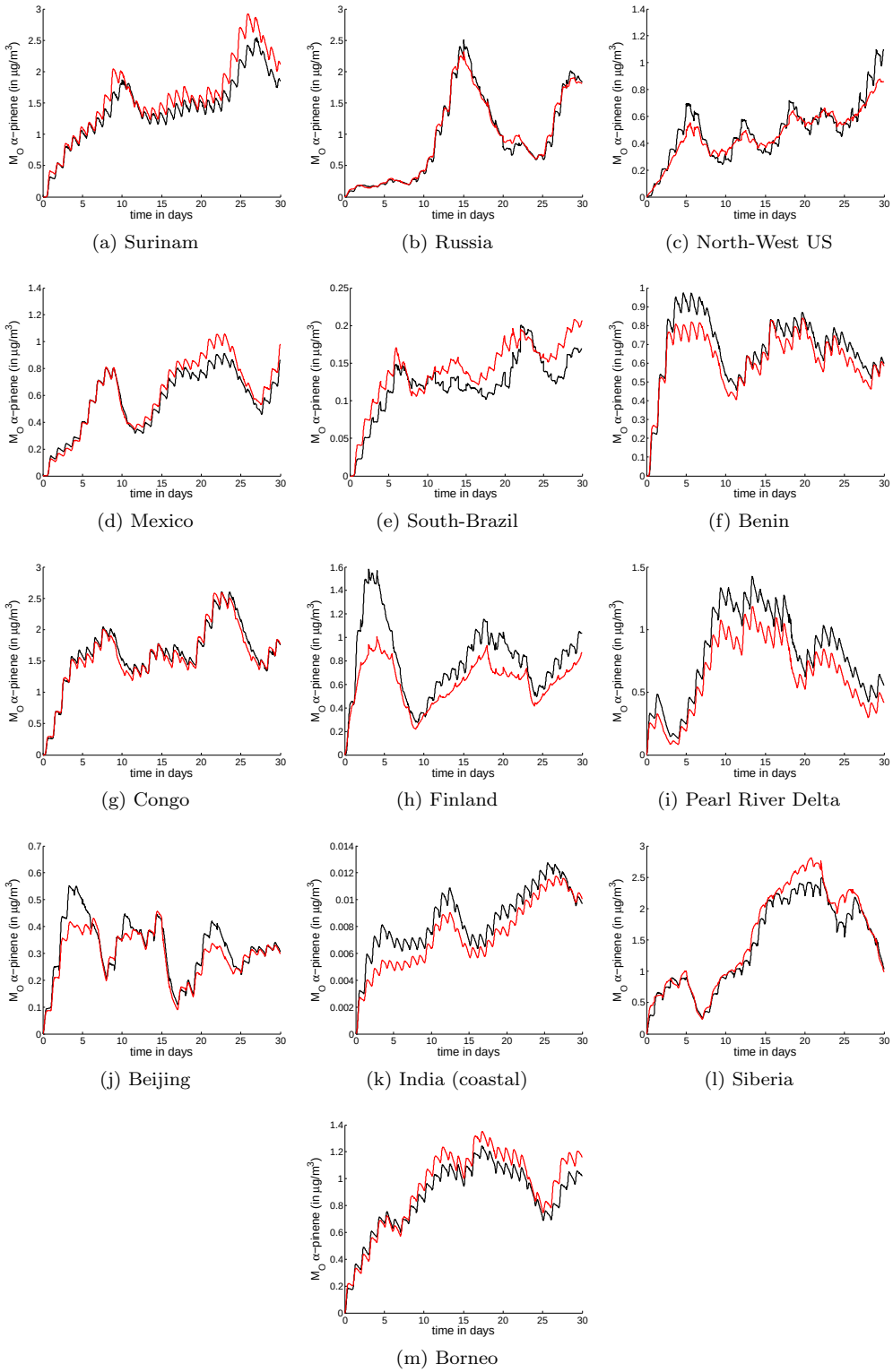

(a) Surinam (b) Russia (c) North-West US

(d) Mexico (e) South-Brazil (f) Benin

(g) Congo (h) Finland (i) Pearl River Delta

(j) Beijing (k) India (coastal) (l) Siberia

(m) Borneo

Figure S17: Example of time evolution of α-pinene SOA in the full BOREAM model (black) versus the parameter model (red) for simulations based on atmospheric conditions simulated with the CTM IMAGESv2, shown here for the month of July.

S6 Parameterised activity coefficients for the 10-product model

γ_{H_2O} (activity coefficient of water, Table S12) and γ_{Org} (pseudo-activity coefficient of the organic SOA fraction, Table S13) are given at RH-values from 0 up to 99.9% for the five scenarios considered.

Table S12: Activity coefficient γ_{H_2O} for water

RH (in %)	γ_{H_2O} OH low-NO_x	γ_{H_2O} OH high-NO_x	γ_{H_2O} O_3 low-NO_x	γ_{H_2O} O_3 high-NO_x	γ_{H_2O} NO_3 high-NO_x
0.0	0.3816	0.5191	0.4470	0.5191	0.5131
1.0	0.3946	0.5291	0.4753	0.5291	0.5232
2.0	0.4072	0.5390	0.4860	0.5390	0.5332
3.0	0.4196	0.5489	0.4965	0.5489	0.5431
4.0	0.4318	0.5586	0.5070	0.5586	0.5529
5.0	0.4437	0.5682	0.5172	0.5682	0.5626
6.0	0.4554	0.5778	0.5274	0.5778	0.5723
7.0	0.4669	0.5873	0.5374	0.5873	0.5818
8.0	0.4783	0.5966	0.5474	0.5966	0.5913
9.0	0.4894	0.6059	0.5572	0.6059	0.6006
10.0	0.5004	0.6151	0.5669	0.6151	0.6099
11.0	0.5113	0.6243	0.5766	0.6243	0.6191
12.0	0.5220	0.6334	0.5861	0.6334	0.6283
13.0	0.5326	0.6424	0.5955	0.6424	0.6373
14.0	0.5430	0.6513	0.6049	0.6513	0.6463
15.0	0.5534	0.6602	0.6141	0.6602	0.6552
16.0	0.5636	0.6689	0.6233	0.6689	0.6641
17.0	0.5737	0.6777	0.6324	0.6777	0.6729
18.0	0.5837	0.6863	0.6414	0.6863	0.6816
19.0	0.5935	0.6949	0.6503	0.6949	0.6902
20.0	0.6033	0.7034	0.6591	0.7034	0.6988
21.0	0.6130	0.7119	0.6679	0.7119	0.7073
22.0	0.6226	0.7203	0.6766	0.7203	0.7158
23.0	0.6321	0.7287	0.6852	0.7287	0.7242
24.0	0.6415	0.7369	0.6937	0.7369	0.7325
25.0	0.6508	0.7451	0.7022	0.7451	0.7408
26.0	0.6600	0.7533	0.7106	0.7533	0.7490
27.0	0.6691	0.7614	0.7189	0.7614	0.7572
28.0	0.6782	0.7695	0.7272	0.7695	0.7653
29.0	0.6872	0.7774	0.7354	0.7774	0.7733
30.0	0.6961	0.7854	0.7435	0.7854	0.7813
31.0	0.7049	0.7933	0.7515	0.7933	0.7892
32.0	0.7136	0.8011	0.7595	0.8011	0.7971
33.0	0.7223	0.8088	0.7674	0.8088	0.8049
34.0	0.7309	0.8165	0.7753	0.8165	0.8127
35.0	0.7394	0.8242	0.7831	0.8242	0.8204
36.0	0.7479	0.8318	0.7908	0.8318	0.8280
37.0	0.7563	0.8393	0.7984	0.8393	0.8356
38.0	0.7646	0.8468	0.8060	0.8468	0.8431
39.0	0.7728	0.8542	0.8136	0.8542	0.8506
40.0	0.7810	0.8616	0.8210	0.8616	0.8580
41.0	0.7891	0.8689	0.8284	0.8689	0.8654
42.0	0.7971	0.8761	0.8357	0.8761	0.8727
43.0	0.8051	0.8833	0.8430	0.8833	0.8800
44.0	0.8129	0.8905	0.8502	0.8905	0.8872
45.0	0.8208	0.8976	0.8573	0.8976	0.8943
46.0	0.8285	0.9046	0.8644	0.9046	0.9014
47.0	0.8362	0.9116	0.8714	0.9116	0.9084
48.0	0.8438	0.9185	0.8783	0.9185	0.9154
49.0	0.8514	0.9253	0.8852	0.9253	0.9223
50.0	0.8589	0.9321	0.8920	0.9321	0.9291
51.0	0.8663	0.9388	0.8987	0.9388	0.9359

Continued on Next Page...

Table S12 – Continued

RH (in %)	γ_{H_2O} OH low-NO_x	γ_{H_2O} OH high-NO_x	γ_{H_2O} O_3 low-NO_x	γ_{H_2O} O_3 high-NO_x	γ_{H_2O} NO_3 high-NO_x
52.0	0.8736	0.9455	0.9054	0.9455	0.9426
53.0	0.8809	0.9521	0.9120	0.9521	0.9493
54.0	0.8881	0.9587	0.9185	0.9587	0.9559
55.0	0.8953	0.9652	0.9249	0.9652	0.9625
56.0	0.9023	0.9716	0.9313	0.9716	0.9689
57.0	0.9093	0.9779	0.9376	0.9779	0.9754
58.0	0.9162	0.9842	0.9438	0.9842	0.9817
59.0	0.9231	0.9904	0.9499	0.9904	0.9880
60.0	0.9298	0.9966	0.9560	0.9966	0.9942
61.0	0.9365	1.0026	0.9620	1.0026	1.0003
62.0	0.9431	1.0086	0.9679	1.0086	1.0064
63.0	0.9497	1.0146	0.9737	1.0146	1.0124
64.0	0.9561	1.0204	0.9795	1.0204	1.0183
65.0	0.9625	1.0262	0.9851	1.0262	1.0241
66.0	0.9688	1.0319	0.9907	1.0319	1.0299
67.0	0.9749	1.0375	0.9961	1.0375	1.0355
68.0	0.9810	1.0430	1.0015	1.0430	1.0411
69.0	0.9871	1.0484	1.0067	1.0484	1.0466
70.0	0.9930	1.0537	1.0119	1.0537	1.0520
71.0	0.9988	1.0590	1.0169	1.0590	1.0573
72.0	1.0045	1.0641	1.0218	1.0641	1.0626
73.0	1.0101	1.0692	1.0267	1.0692	1.0676
74.0	1.0156	1.0741	1.0313	1.0741	1.0727
75.0	1.0209	1.0789	1.0359	1.0789	1.0775
76.0	1.0262	1.0836	1.0403	1.0836	1.0823
77.0	1.0313	1.0881	1.0446	1.0881	1.0869
78.0	1.0363	1.0926	1.0487	1.0926	1.0915
79.0	1.0411	1.0969	1.0526	1.0969	1.0958
80.0	1.0458	1.1010	1.0564	1.1010	1.1000
80.5	1.0480	1.1030	1.0582	1.1030	1.1021
81.0	1.0503	1.1050	1.0600	1.1050	1.1041
81.5	1.0524	1.1069	1.0617	1.1069	1.1061
82.0	1.0546	1.1088	1.0633	1.1088	1.1080
82.5	1.0567	1.1106	1.0649	1.1106	1.1099
83.0	1.0587	1.1124	1.0665	1.1124	1.1117
83.5	1.0607	1.1141	1.0679	1.1141	1.1135
84.0	1.0626	1.1158	1.0694	1.1158	1.1152
84.5	1.0645	1.1175	1.0707	1.1175	1.1169
85.0	1.0663	1.1190	1.0720	1.1190	1.1185
85.5	1.0680	1.1205	1.0732	1.1205	1.1200
86.0	1.0697	1.1220	1.0743	1.1220	1.1215
86.5	1.0713	1.1234	1.0753	1.1234	1.1229
87.0	1.0729	1.1247	1.0762	1.1247	1.1243
87.5	1.0743	1.1259	1.0771	1.1259	1.1256
88.0	1.0757	1.1271	1.0778	1.1271	1.1268
88.5	1.0769	1.1281	1.0784	1.1281	1.1279
89.0	1.0781	1.1291	1.0789	1.1291	1.1289
89.5	1.0792	1.1300	1.0792	1.1300	1.1299
90.0	1.0801	1.1308	1.0794	1.1308	1.1307
90.5	1.0809	1.1314	1.0795	1.1314	1.1315
91.0	1.0816	1.1320	1.0793	1.1320	1.1321
91.5	1.0821	1.1324	1.0790	1.1324	1.1325
92.0	1.0824	1.1327	1.0784	1.1327	1.1329
92.5	1.0826	1.1328	1.0776	1.1328	1.1331
93.0	1.0825	1.1327	1.0764	1.1327	1.1331
93.5	1.0822	1.1325	1.0749	1.1325	1.1329
94.0	1.0816	1.1320	1.0730	1.1320	1.1325
94.5	1.0806	1.1312	1.0707	1.1312	1.1319
95.0	1.0792	1.1302	1.0676	1.1302	1.1310

Continued on Next Page...

Table S12 – Continued

RH (in %)	γ_{H_2O} OH low-NO_x	γ_{H_2O} OH high-NO_x	γ_{H_2O} O_3 low-NO_x	γ_{H_2O} O_3 high-NO_x	γ_{H_2O} NO_3 high-NO_x
95.1	1.0788	1.1300	1.0669	1.1300	1.1307
95.2	1.0784	1.1297	1.0662	1.1297	1.1305
95.3	1.0780	1.1294	1.0655	1.1294	1.1302
95.4	1.0776	1.1291	1.0647	1.1291	1.1300
95.5	1.0772	1.1288	1.0638	1.1288	1.1297
95.6	1.0767	1.1285	1.0629	1.1285	1.1294
95.7	1.0762	1.1281	1.0620	1.1281	1.1291
95.8	1.0757	1.1278	1.0610	1.1278	1.1287
95.9	1.0751	1.1274	1.0600	1.1274	1.1284
96.0	1.0745	1.1270	1.0589	1.1270	1.1280
96.1	1.0739	1.1266	1.0578	1.1266	1.1276
96.2	1.0732	1.1261	1.0566	1.1261	1.1272
96.3	1.0725	1.1257	1.0554	1.1257	1.1268
96.4	1.0717	1.1252	1.0540	1.1252	1.1263
96.5	1.0709	1.1247	1.0526	1.1247	1.1259
96.6	1.0700	1.1241	1.0511	1.1241	1.1254
96.7	1.0691	1.1236	1.0495	1.1236	1.1248
96.8	1.0681	1.1230	1.0478	1.1230	1.1243
96.9	1.0670	1.1223	1.0460	1.1223	1.1237
97.0	1.0659	1.1217	1.0441	1.1217	1.1231
97.1	1.0646	1.1210	1.0421	1.1210	1.1224
97.2	1.0633	1.1202	1.0400	1.1202	1.1218
97.3	1.0618	1.1195	1.0377	1.1195	1.1210
97.4	1.0602	1.1186	1.0353	1.1186	1.1203
97.5	1.0585	1.1178	1.0328	1.1178	1.1195
97.6	1.0565	1.1168	1.0301	1.1168	1.1186
97.7	1.0544	1.1159	1.0274	1.1159	1.1177
97.8	1.0520	1.1148	1.0247	1.1148	1.1167
97.9	1.0492	1.1137	1.0220	1.1137	1.1157
98.0	1.0460	1.1125	1.0194	1.1125	1.1146
98.1	1.0423	1.1112	1.0169	1.1112	1.1135
98.2	1.0379	1.1099	1.0146	1.1099	1.1122
98.3	1.0327	1.1084	1.0125	1.1084	1.1109
98.4	1.0268	1.1068	1.0106	1.1068	1.1094
98.5	1.0208	1.1050	1.0089	1.1050	1.1078
98.6	1.0158	1.1031	1.0074	1.1031	1.1061
98.7	1.0120	1.1010	1.0061	1.1010	1.1042
98.8	1.0091	1.0985	1.0050	1.0985	1.1021
98.9	1.0069	1.0957	1.0041	1.0957	1.0998
99.0	1.0052	1.0924	1.0032	1.0924	1.0971
99.1	1.0039	1.0079	1.0025	1.0079	1.0099
99.2	1.0029	1.0049	1.0019	1.0049	1.0056
99.3	1.0021	1.0032	1.0014	1.0032	1.0035
99.4	1.0014	1.0021	1.0010	1.0021	1.0022
99.5	1.0010	1.0013	1.0007	1.0013	1.0014
99.6	1.0006	1.0008	1.0004	1.0008	1.0008
99.7	1.0003	1.0004	1.0002	1.0004	1.0004
99.8	1.0001	1.0002	1.0001	1.0002	1.0002
99.9	1.0000	1.0000	1.0000	1.0000	1.0000

Table S13: Pseudo-activity coefficient γ_{Org} for impact of water on the organic fraction

RH (in %)	γ_{Org} OH low-NO_x	γ_{Org} OH high-NO_x	γ_{Org} O_3 low-NO_x	γ_{Org} O_3 high-NO_x	γ_{Org} NO_3 high-NO_x
0.0	1.0000	1.0000	1.0000	1.0000	1.0000
1.0	0.9996	0.9998	0.9993	0.9998	0.9998
2.0	0.9983	0.9993	0.9986	0.9993	0.9993
3.0	0.9964	0.9984	0.9975	0.9984	0.9984
4.0	0.9939	0.9972	0.9959	0.9972	0.9971
5.0	0.9908	0.9958	0.9940	0.9958	0.9956
6.0	0.9872	0.9940	0.9917	0.9940	0.9938
7.0	0.9832	0.9920	0.9891	0.9920	0.9917
8.0	0.9787	0.9897	0.9862	0.9897	0.9894
9.0	0.9739	0.9872	0.9830	0.9872	0.9868
10.0	0.9688	0.9844	0.9796	0.9844	0.9840
11.0	0.9634	0.9815	0.9759	0.9815	0.9809
12.0	0.9577	0.9783	0.9719	0.9783	0.9777
13.0	0.9517	0.9749	0.9678	0.9749	0.9742
14.0	0.9455	0.9714	0.9634	0.9714	0.9706
15.0	0.9391	0.9677	0.9589	0.9677	0.9668
16.0	0.9326	0.9638	0.9541	0.9638	0.9628
17.0	0.9258	0.9597	0.9492	0.9597	0.9587
18.0	0.9189	0.9556	0.9442	0.9556	0.9544
19.0	0.9119	0.9512	0.9389	0.9512	0.9500
20.0	0.9047	0.9467	0.9336	0.9467	0.9454
21.0	0.8974	0.9421	0.9281	0.9421	0.9407
22.0	0.8900	0.9374	0.9224	0.9374	0.9358
23.0	0.8825	0.9325	0.9167	0.9325	0.9309
24.0	0.8749	0.9276	0.9109	0.9276	0.9258
25.0	0.8672	0.9225	0.9049	0.9225	0.9207
26.0	0.8595	0.9173	0.8988	0.9173	0.9154
27.0	0.8517	0.9121	0.8927	0.9121	0.9100
28.0	0.8438	0.9067	0.8865	0.9067	0.9046
29.0	0.8359	0.9013	0.8801	0.9013	0.8990
30.0	0.8280	0.8958	0.8738	0.8958	0.8934
31.0	0.8200	0.8901	0.8673	0.8901	0.8877
32.0	0.8119	0.8844	0.8608	0.8844	0.8819
33.0	0.8039	0.8787	0.8542	0.8787	0.8760
34.0	0.7958	0.8729	0.8475	0.8729	0.8701
35.0	0.7876	0.8670	0.8408	0.8670	0.8641
36.0	0.7795	0.8610	0.8341	0.8610	0.8581
37.0	0.7714	0.8550	0.8273	0.8550	0.8520
38.0	0.7632	0.8490	0.8204	0.8490	0.8458
39.0	0.7550	0.8429	0.8135	0.8429	0.8396
40.0	0.7469	0.8367	0.8066	0.8367	0.8334
41.0	0.7387	0.8305	0.7997	0.8305	0.8270
42.0	0.7306	0.8243	0.7927	0.8243	0.8207
43.0	0.7224	0.8180	0.7857	0.8180	0.8143
44.0	0.7142	0.8117	0.7787	0.8117	0.8079
45.0	0.7061	0.8053	0.7716	0.8053	0.8015
46.0	0.6980	0.7990	0.7646	0.7990	0.7950
47.0	0.6899	0.7925	0.7575	0.7925	0.7885
48.0	0.6818	0.7861	0.7504	0.7861	0.7820
49.0	0.6737	0.7796	0.7433	0.7796	0.7754
50.0	0.6656	0.7732	0.7362	0.7732	0.7689
51.0	0.6576	0.7667	0.7290	0.7667	0.7623
52.0	0.6496	0.7601	0.7219	0.7601	0.7557
53.0	0.6416	0.7536	0.7148	0.7536	0.7491
54.0	0.6337	0.7471	0.7077	0.7471	0.7425
55.0	0.6257	0.7405	0.7005	0.7405	0.7358
56.0	0.6179	0.7340	0.6934	0.7340	0.7292
57.0	0.6100	0.7274	0.6863	0.7274	0.7225

Continued on Next Page...

Table S13 – Continued

RH (in %)	γ_{Org} OH low-NO_x	γ_{Org} OH high-NO_x	γ_{Org} O_3 low-NO_x	γ_{Org} O_3 high-NO_x	γ_{Org} NO_3 high-NO_x
58.0	0.6022	0.7208	0.6792	0.7208	0.7159
59.0	0.5944	0.7143	0.6721	0.7143	0.7092
60.0	0.5867	0.7077	0.6651	0.7077	0.7026
61.0	0.5789	0.7011	0.6580	0.7011	0.6959
62.0	0.5713	0.6946	0.6510	0.6946	0.6893
63.0	0.5637	0.6880	0.6440	0.6880	0.6827
64.0	0.5561	0.6815	0.6370	0.6815	0.6761
65.0	0.5486	0.6750	0.6300	0.6750	0.6695
66.0	0.5411	0.6685	0.6231	0.6685	0.6629
67.0	0.5337	0.6620	0.6162	0.6620	0.6564
68.0	0.5263	0.6555	0.6093	0.6555	0.6498
69.0	0.5190	0.6491	0.6025	0.6491	0.6433
70.0	0.5118	0.6427	0.5958	0.6427	0.6369
71.0	0.5046	0.6363	0.5890	0.6363	0.6304
72.0	0.4975	0.6300	0.5824	0.6300	0.6240
73.0	0.4904	0.6238	0.5758	0.6238	0.6177
74.0	0.4834	0.6175	0.5693	0.6175	0.6114
75.0	0.4765	0.6113	0.5628	0.6113	0.6051
76.0	0.4697	0.6052	0.5565	0.6052	0.5990
77.0	0.4630	0.5992	0.5503	0.5992	0.5929
78.0	0.4564	0.5933	0.5441	0.5933	0.5868
79.0	0.4499	0.5874	0.5381	0.5874	0.5809
80.0	0.4435	0.5816	0.5323	0.5816	0.5751
80.5	0.4403	0.5788	0.5294	0.5788	0.5722
81.0	0.4372	0.5760	0.5266	0.5760	0.5694
81.5	0.4341	0.5732	0.5238	0.5732	0.5666
82.0	0.4311	0.5705	0.5211	0.5705	0.5638
82.5	0.4281	0.5678	0.5184	0.5678	0.5611
83.0	0.4251	0.5651	0.5158	0.5651	0.5584
83.5	0.4222	0.5625	0.5133	0.5625	0.5557
84.0	0.4194	0.5600	0.5109	0.5600	0.5531
84.5	0.4166	0.5575	0.5085	0.5575	0.5506
85.0	0.4138	0.5550	0.5062	0.5550	0.5481
85.5	0.4111	0.5527	0.5040	0.5527	0.5457
86.0	0.4085	0.5504	0.5020	0.5504	0.5433
86.5	0.4060	0.5481	0.5000	0.5481	0.5410
87.0	0.4036	0.5460	0.4982	0.5460	0.5388
87.5	0.4012	0.5439	0.4966	0.5439	0.5367
88.0	0.3989	0.5419	0.4951	0.5419	0.5346
88.5	0.3968	0.5401	0.4939	0.5401	0.5327
89.0	0.3948	0.5384	0.4929	0.5384	0.5309
89.5	0.3930	0.5368	0.4921	0.5368	0.5293
90.0	0.3913	0.5353	0.4916	0.5353	0.5278
90.5	0.3898	0.5341	0.4916	0.5341	0.5264
91.0	0.3885	0.5331	0.4919	0.5331	0.5253
91.5	0.3875	0.5323	0.4928	0.5323	0.5243
92.0	0.3868	0.5317	0.4943	0.5317	0.5237
92.5	0.3865	0.5315	0.4965	0.5315	0.5233
93.0	0.3867	0.5316	0.4998	0.5316	0.5233
93.5	0.3875	0.5322	0.5043	0.5322	0.5236
94.0	0.3889	0.5333	0.5105	0.5333	0.5245
94.5	0.3913	0.5350	0.5189	0.5350	0.5260
95.0	0.3950	0.5376	0.5304	0.5376	0.5282
95.1	0.3960	0.5382	0.5332	0.5382	0.5288
95.2	0.3970	0.5388	0.5362	0.5388	0.5294
95.3	0.3981	0.5395	0.5394	0.5395	0.5300
95.4	0.3992	0.5403	0.5429	0.5403	0.5307
95.5	0.4005	0.5411	0.5466	0.5411	0.5314
95.6	0.4019	0.5420	0.5507	0.5420	0.5322

Continued on Next Page...

Table S13 – Continued

RH (in %)	γ_{Org} OH low-NO_x	γ_{Org} OH high-NO_x	γ_{Org} O_3 low-NO_x	γ_{Org} O_3 high-NO_x	γ_{Org} NO_3 high-NO_x
95.7	0.4034	0.5429	0.5550	0.5429	0.5330
95.8	0.4050	0.5439	0.5597	0.5439	0.5339
95.9	0.4067	0.5449	0.5648	0.5449	0.5348
96.0	0.4086	0.5460	0.5703	0.5460	0.5358
96.1	0.4107	0.5472	0.5763	0.5472	0.5369
96.2	0.4129	0.5485	0.5829	0.5485	0.5380
96.3	0.4153	0.5498	0.5901	0.5498	0.5392
96.4	0.4179	0.5512	0.5981	0.5512	0.5405
96.5	0.4208	0.5527	0.6069	0.5527	0.5418
96.6	0.4240	0.5544	0.6166	0.5544	0.5433
96.7	0.4275	0.5561	0.6274	0.5561	0.5448
96.8	0.4313	0.5579	0.6396	0.5579	0.5465
96.9	0.4356	0.5599	0.6532	0.5599	0.5483
97.0	0.4403	0.5620	0.6687	0.5620	0.5502
97.1	0.4456	0.5643	0.6862	0.5643	0.5522
97.2	0.4516	0.5667	0.7063	0.5667	0.5544
97.3	0.4584	0.5693	0.7294	0.5693	0.5567
97.4	0.4661	0.5721	0.7561	0.5721	0.5593
97.5	0.4750	0.5752	0.7870	0.5752	0.5620
97.6	0.4855	0.5784	0.8228	0.5784	0.5649
97.7	0.4979	0.5820	0.8643	0.5820	0.5681
97.8	0.5129	0.5859	0.9120	0.5859	0.5715
97.9	0.5315	0.5901	0.9663	0.5901	0.5752
98.0	0.5552	0.5947	1.0274	0.5947	0.5793
98.1	0.5864	0.5998	1.0952	0.5998	0.5838
98.2	0.6295	0.6055	1.1691	0.6055	0.5887
98.3	0.6917	0.6118	1.2488	0.6118	0.5941
98.4	0.7826	0.6189	1.3335	0.6189	0.6002
98.5	0.9058	0.6269	1.4229	0.6269	0.6070
98.6	1.0512	0.6361	1.5165	0.6361	0.6147
98.7	1.2059	0.6468	1.6140	0.6468	0.6235
98.8	1.3638	0.6594	1.7153	0.6594	0.6337
98.9	1.5235	0.6748	1.8203	0.6748	0.6458
99.0	1.6851	0.6944	1.9288	0.6944	0.6604
99.1	1.8490	10.9435	2.0411	10.9435	8.4866
99.2	2.0161	13.3715	2.1571	13.3715	11.0986
99.3	2.1870	15.5159	2.2771	15.5159	13.1790
99.4	2.3625	17.5656	2.4015	17.5656	15.1215
99.5	2.5432	19.5864	2.5306	19.5864	17.0209
99.6	2.7304	21.6130	2.6651	21.6130	18.9197
99.7	2.9257	23.6717	2.8064	23.6717	20.8464
99.8	3.1331	25.8010	2.9574	25.8010	22.8372
99.9	3.1331	25.8010	2.9574	25.8010	22.8372

S7 Comparison of the parameterisation for RH-dependence at intermediate NO_x

The following figure compares the full BOREAM model and the parameterisation for total SOA mass concentration (including water) as a function of relative humidity (RH) at 2 intermediate NO_x levels. Also shown are results for 2 sensitivity tests for which activity coefficients are constant and equal to 1 (ideality). This assumption leads to significant discrepancies at higher RH values .

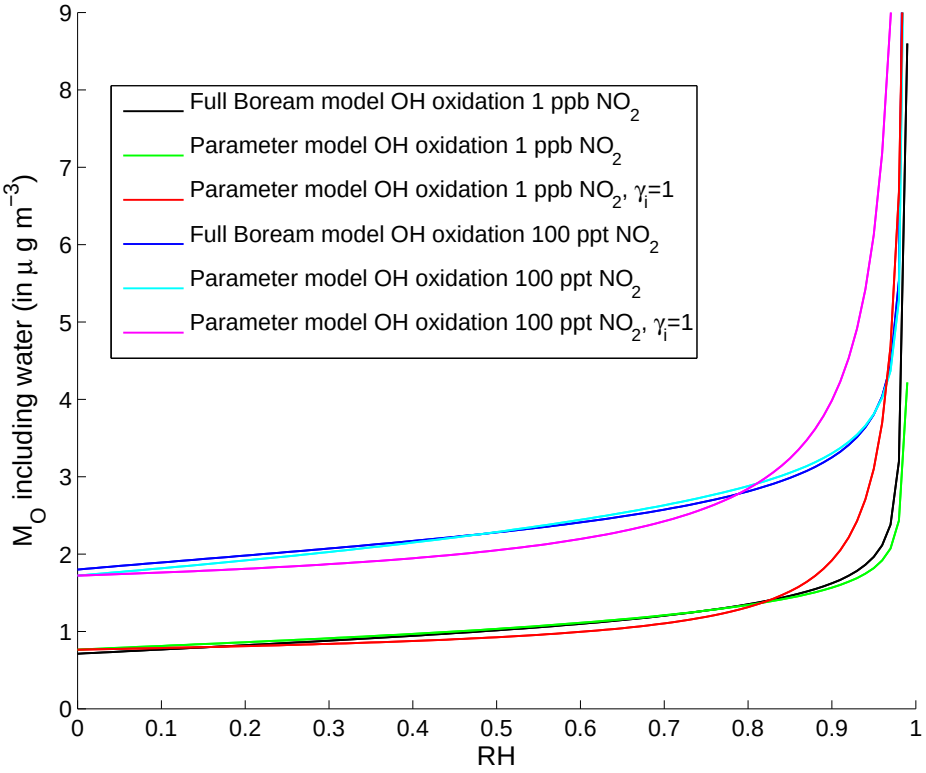

Figure S18: Parameterised and full model SOA mass loading M_O (including water) in function of RH, at 100 ppt and 1 ppb NO_2 for the OH-oxidation scenario (at 288 K). Also shown are results for 2 sensitivity tests for which activity coefficients are constant and equal to 1 (ideality).

References

Atkinson, R. et al.: Evaluated kinetic and photochemical data for atmospheric chemistry: Volume II - gas phase reactions of organic species, Atmos. Chem. Phys., 6, 3625–4055, 2006.

Capouet, M. and Müller, J.-F.: A group contribution method for estimating the vapour pressures of α-pinene oxidation products, Atmos. Chem. Phys., 6, 1455–1467, doi:10.5194/acp-6-1455-2006, 2006.

Capouet, M., Peeters, J., Nozière, B., and Müller, J.-F.: α-pinene oxidation by OH: simulations of laboratory experiments, Atmos. Chem. Phys., 4, 2285–2311, doi:10.5194/acp-4-2285-2004, 2004.

Capouet, M., Müller, J.-F., Ceulemans, K., Compernolle, S., Vereecken, L., and Peeters, J.: Modeling aerosol formation in α-pinene photo-oxidation experiments, J. Geophys. Res., 113, D02 308, doi:10.1029/2007JD008995, 2008.

Carter, W. P. L.: Documentation of the SAPRC-99 chemical mechanism for VOC reactivity assessment, final report to California Air Resources Board, contracts 92-329 and 95-308,

Tech. rep., Air Pollut. Res. Cent.for Environ. Res. and Technol., Univ. of California, Riverside, California, URL `http://.www.cert.ucr.edu/ carter/reactdat.htm`, 2000.

Ceulemans, K., Compernolle, S., Peeters, J., and Müller, J.-F.: Evaluation of a detailed model of secondary organic aerosol formation from α-pinene against dark ozonolysis experiments, Atmos. Environ., 44, 5434–5442, doi:10.5194/acp-9-1325-2009, 2010.

Jenkin, M. E., Hurley, M. D., and Wallington, T. J.: Investigation of the radical product channel of the $CH_3C(O)O_2$ + HO_2 reaction in the gas phase, Phys. Chem. Chem. Phys., 9, 3149–3162, 2007.

Makar, P. A.: The estimation of organic gas vapour pressure, Atmos. Environ., 35, 961–974, 2001.

Neeb, P.: Structure-reactivity based estimation of the rate constants for hydroxyl radical reactions with hydrocarbons, J. Atmos. Chem., 35, 295–315, 2000.

Ng, N. L., Chhabra, P. S., Chan, A. W. H., Surratt, J. D., Kroll, J. H., Kwan, A. J., McCabe, D. C., Wennberg, P. O., Sorooshian, A., Murphy, S. M., Dalleska, N. F., Flagan, R. C., and Seinfeld, J. H.: Effect of NO_x level on secondary organic aerosol (SOA) formation from the photooxidation of terpenes, Atmos. Chem. Phys., 7, 5159–5174, doi:10.5194/acp-7-5159-2007, 2007.

Paulson, S. E., Liu, D.-L., and Orzechowska, G. E.: Photolysis of heptanal, J. Org. Chem., 71, 6403–6408, 2006.

Saunders, S. M., Jenkin, M. E., Derwent, R. G., and Pilling, M. J.: Protocol for the development of the Master Chemical Mechanism, MCM v3 (Part A): tropospheric degradation of non-aromatic volatile organic compounds, Atmos. Chem. Phys., 3, 161–180, 2003.

Schurath, U. and Naumann, K.-H.: Chemical Mechanism Develoment (CMD), EUROTRAC-2 subproject, final report, Tech. rep., Int. Sci. Secr.t, GSF-Natl. Res. Cent. for Environ. and Health, Munich, Germany, 2003.

Valorso, R., Aumont, B., Camredon, M., Raventos-Duran, T., Mouchel-Vallon, C., Ng, N. L., Seinfeld, J. H., Lee-Taylor, J., and Madronich, S.: Explicit modelling of SOA formation from α-pinene photooxidation: sensitivity to vapour pressure estimation, Atmos. Chem. Phys., 11, 68956910, doi:10.5194/acp-11-6895-2011, 2011.

Vereecken, L. and Peeters, J.: Decomposition of substituted alkoxy radicals - part 1: a generalized structure-activity relationship for reaction barrier heights, Phys. Chem. Chem. Phys., 11, 9062–9074, 2009.